Journal Pre-proof

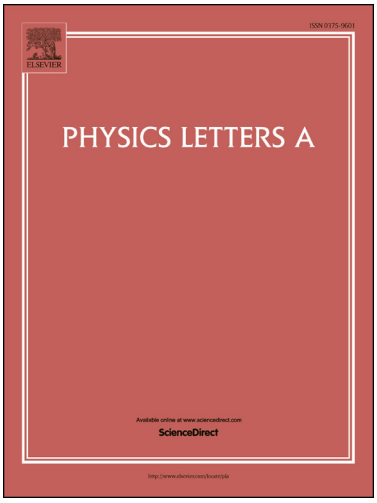

Beyond the Vegard's law: solid mixing excess volume and thermodynamic potentials prediction, from end-members

Marcello Merli, Alessandro Pavese

PII: S0375-9601(19)30948-X
DOI: https://doi.org/10.1016/j.physleta.2019.126059
Reference: PLA 126059

To appear in: *Physics Letters A*

Received date: 13 May 2019
Revised date: 3 October 2019
Accepted date: 10 October 2019

Please cite this article as: M. Merli, A. Pavese, Beyond the Vegard's law: solid mixing excess volume and thermodynamic potentials prediction, from end-members, *Phys. Lett. A* (2019), 126059, doi: https://doi.org/10.1016/j.physleta.2019.126059.

Highlights

- The Energy and Volumes data are obtained via first principles modelling.
- The state functions, $E(V,T)$s, of each end members are expanded in a polynomial basis in V_{Mix} (the volume of the solid solution) and linearly summed in Vegard's scheme.
- V_{Mix} is determined by solving the fundamental equilibrium equation $-(\partial E/\partial V)_T = P$.
- Consequentely, EMIX and all the excess functions can be easily derived.

Beyond the Vegard's law: solid mixing excess volume and thermodynamic potentials prediction, from end-members

Marcello Merli[1a] and Alessandro Pavese[2]

[1]Department of Earth and Sea Sciences (DiSTeM), University of Palermo – Via Archirafi 36 – 90123 Palermo – Italy

[2] Earth Sciences Department – University of Turin – Via Valperga Caluso 35 – 10100 Turin – Italy

[a]To whom correspondence should be addressed. Email address: marcello.merli@unipa.it

Abstract

A method has been developed, herein presented, to model binary solid solutions' volume, enthalpy and Gibbs energy using the energy state functions, $E(V,S)$, of the end-members only. The $E(V,S)s$ are expanded around an unknown mixing volume, V_{Mix}, and the fundamental equilibrium equation $-(\partial E/\partial V)_S = P$ is used to determine V_{Mix}. V_{Mix} allows us to model enthalpy, straightforwardly. The same argument holds using Helmholtz energy, $F(V,T)$, in place of $E(V,S)$, and the equilibrium equation becomes $-(\partial F/\partial V)_T = P$. One can readily determine the Gibbs free energy, too. The method presented remarkably simplifies computing of solid mixings' thermodynamic properties and makes it possible to preserve crystal structure symmetry that would undergo reduction because of the introduction of disordered super-cells.

Keywords

Thermodynamic modeling, Computer simulations, Metals and alloys, Nitride materials

1. Introduction

Solid mixing is a common phenomenology occurring in crystals and affecting their properties and stability. Mineralogy, metallurgy and materials science deal with crystalline solids, which have structures characterized by isomorphic atomic replacements, often involving more than two end-members. Dating back to Vegard, treating solid mixings by means only of their end-members (EM) has been an object of interest, both for the scientific implications and the relevant simplifications that would ensue in performing calculations [1]. Jacob et al. critically revised the notion of Vegard-type linearity between a solid solution and its EMs, paying special attention to whether such a relationship is a bare, though effective and efficient, approximation or it expresses a fundamental relation [2].

An early model to predict lattice parameters of an alloy as a function of the composition was proposed by Moreen et al., who based their method on the assumption that lattice parameters of solid solutions are the average of all the interatomic distances over a selected and representative portion of lattice [3]. Denton and Ashcroft pointed out the role of the atomic sizes to allow formation of a solid mixing [4]. The “Delta Lattice Parameter” (DLP) model of Stringfellow for calculation of excess enthalpy relies on the lattice mismatch between solid mixing and EMs, assuming a regular (symmetric) behaviour of the resulting solid solution [5]. In the early seventies, the “Coherent Potential Approximation” (CPA) was extended to random materials through the Korringa, Kohn and Rostoker (KKR) method, thus making it possible to model the energetics of a disordered material [6]. The Connolly-Williams (CW) method resorts to the determination of effective cluster interactions (ECIs) from the formation enthalpies of a set of reference ordered structures [7]. ECIs, in turn, allow an estimate of alloys’ formation enthalpies. The “Special Quasi-random Structures” (SQSs) technique uses supercells to model a random configuration of atoms. All the mentioned methods assume that the energy of an alloy can be expressed via cluster expansions. The Cluster Expansion method [8] (see [9] for a review. In the case of applications to natural systems, see [10,11]) allows one to exploit a theoretically robust approach, which makes it possible to explore the properties of solid mixings even at extreme conditions, though at exceedingly demanding computing costs [12,13]. In fact, the “cluster

expansion method" requires investigation of as many configurations as possible, resorting to super cells to mimic atomic disorder in a crystal. Moreover, all this implies an unavoidable breakdown of the crystal symmetry, as a function of the configuration under study. The Virtual Crystal Approximation (VCA) provides an alternative approach based on a solid mixing description that employs the notion of site occupancy, i.e. the probability of having a given species at a crystal site [14,15]. Although such a method preserves crystal symmetry and allows one to avoid using super-cells, yet it simply represents the transposition of the Vegard's law to the microscopic scale. In "Critical analysis of the virtual crystal approximation" by Dargam et. al., the authors point out the limits and drawbacks related to the use of VCA [15]. In general, modelling of solid mixings has attracted the interest of several authors, who resorted to a variety of approaches, often chosen as a function of the observables they meant to reproduce. In [12,16] the reader can find a survey upon such a subject. Recent papers also demonstrate a lively interest in excess properties of liquid phases, in particular about volume excess, even at non-ambient conditions [17,18,19,20].

Although the "cluster expansion method" is robustly formulated, it implies many difficulties because of the complexity one faces in providing a faithful representation of a solid mixing, in terms of i) choosing a representative portion of a disordered crystal, i.e. supercell's size determination, and ii) exploring the related disordered atomic arrangements. In this view, being able to infer some fundamental properties of a solid mixing using only the EMs would result in a significant enhancement to modelling and understanding such systems [21,22].

In the present paper, we introduce a binary mixing model that aims to predict solid solutions' volume and thermodynamic potentials (energy, E; Helmholtz energy, F; enthalpy, H; Gibbs energy, G), resorting to EMs only, and using E as a key state function. The model in question is tested by comparing synthetic data produced using quantum mechanics modelling with experimental observations and earlier calculations, on a number of solid mixings.

2. Theoretical background

2.1 Model

The energy E_{Mix} of a solid solution between two phases *A* and *B* can be formulated as

$$E(x)_{Mix} = xE_A + (1-x)E_B + O(x), \quad (1)$$

where *x* is the mole fraction of the component *A* and $O(x) = \sum_{n,m=1,M} C_{nm} x^n (1-x)^m$, with C_{nm} being the coefficients of the M^{th}-degree polynomial function.

E_j is here expressed as a function of volume and entropy, i.e. $E_j = f(V_j, S)$; *j* refers to the j^{th}-phase, i.e. *A* and *B*. Hereafter, we drop *S*, for the sake of simplicity of notation. At a given *S*, E_j can be expanded in terms of powers of V_j, i.e.

$$E_j = \sum_{m=0}^{M} k_{j,m} V_j^m + O\left(V_j^{M+1}\right) \quad (2)$$

with $k_{j,m}$ being the coefficient for the j^{th}-phase of the m^{th}-degree term.

Taking into account that

$$E_{Mix}(V_{Mix}) = x \sum_{m=0}^{M} k_{A,m} V_A^m + (1-x) \sum_{l=0}^{L} k_{B,l} V_B^l + O(x) \quad (3)$$

and setting

1) $V_j = V_{Mix} + \delta$

2) $N = \max\{L, M\}$,

Eq. (3) can be recast into the following expression

$$E_{Mix}(V_{Mix}) = x \sum_{n=0}^{N} k_{A,n} V_{Mix}^n \left(1 + \frac{\delta_A}{V_{Mix}}\right)^n + (1-x) \sum_{n=0}^{N} k_{B,n} V_{Mix}^n \left(1 + \frac{\delta_B}{V_{Mix}}\right)^n + O(x),$$

which is readily turned into

$$E_{Mix}(V_{Mix}) = \sum_{n=0}^{N} [\, x\, k_{A,n} + (1-x) k_{B,n} \,] V_{Mix}^n + \sum_{n=1}^{N} V_{Mix}^n \sum_{r=1}^{n} \binom{n}{r} \left[\left(\frac{\delta_A}{V_{Mix}}\right)^r x\, k_{A,n} + \left(\frac{\delta_B}{V_{Mix}}\right)^r (1-x)\, k_{B,n} \right] + O(x). \quad (4.a)$$

In the equations above V_{Mix} means volume of the solid mixing generated by *A* and *B*; V_{Mix}-V_A-V_B are supposed to be at equilibrium at given and shared *P*-*T* conditions.

The second right-hand side member of Eq. (4.a) depends on powers of

$$\varepsilon_{A,B} = \left(\frac{\delta_{A,B}}{V_{Mix}}\right). \quad (4.b)$$

$\varepsilon_{A,B}$ turns out to be on average as large as ~5%, an estimate we obtained on the basis of the cases explored. In such a view, we altogether assume that the ε-dependent terms of Eq. (4.a) can be neglected, so that the solid mixing energy is expressed as a function of V_{Mix} and *x*, only, i.e.

$$E_{Mix}(V_{Mix}) \approx \sum_{n=0}^{N} [\, x\, k_{A,n} + (1-x) k_{B,n} \,]\, V_{Mix}^{n} + O(x). \quad (5)$$

The legitimacy of such a truncation and the ensuing effects will be discussed in the next section. Let us focus attention on Eq. (5) and the relationship beneath

$$-\left(\frac{\partial E_{Mix}}{\partial V_{Mix}}\right)_{S} = P. \quad (6)$$

A crucial step consists in estimating the following derivative

$$-\left(\frac{\partial O(x)}{\partial V_{Mix}}\right)_{S},$$

which is accomplished as reported below.

We recast Eq. (1) into its differential form, that is

$$dE_{Mix} = x dE_A + (1-x) dE_B + dO(x),$$

where the infinitesimal variations of energy are due to infinitesimal changes of the volumes of the involved phases. We divide and multiply each term of the equation above by the related *dV*. In so doing, one obtains

$$\frac{dE_{Mix}}{dV_{Mix}} dV_{Mix} = x \frac{dE_A}{dV_A} dV_A + (1-x) \frac{dE_B}{dV_B} dV_B + \frac{dO(x)}{dV_{Mix}} dV_{Mix}.$$

Taking into account Eq. (6), the expression above is recast into

$$-P dV_{Mix} = -Px dV_A - (1-x) P dV_B + \frac{dO(x)}{dV_{Mix}} dV_{Mix},$$

from which it descends

$$P[-dV_{Mix} + x dV_A + (1-x) dV_B] = \frac{dO(x)}{dV_{Mix}} dV_{Mix}$$

and eventually

$$P\left(-1 + x \frac{dV_A}{dV_{Mix}} + (1-x) \frac{dV_B}{dV_{Mix}}\right) = \frac{dO(x)}{dV_{Mix}}\,. \quad (7)$$

In Eq. (7), one observes that

$$\frac{dV_A}{dV_{Mix}} = \frac{1}{x + o(x^2)} \approx \frac{1}{x}$$

and

$$\frac{dV_B}{dV_{Mix}} = \frac{1}{1-x+o((1-x)^2)} \approx \frac{1}{1-x}$$

hold.

In view of all this, $\frac{dO(x)}{dV_{Mix}}$ is expected to yield a negligible contribution to *P*, in Eq. (6). Therefore, the solid mixing volume must fulfill the relationship shown below

$$\sum_{n=1}^{N} n\, [\, x\, k_{A,n} + (1-x) k_{B,n} \,]\, V_{Mix}^{n-1} \approx P. \quad (8)$$

From Eq. (8), one is able to obtain V_{Mix} once the roots of the related (n-1)th-order polynomial have been determined. Let us refer to the V_{Mix}-solution of Eq. (8) by $V_{Mix,0}$ and to the physically correct V_{Mix}-value by $V_{Mix,corr}$, so that $V_{Mix,0} = V_{Mix,corr} + \delta V$. One readily reformulates Eq. (8) into

$$\sum_{n=1}^{N} n\,[\,x\,k_{A,n} + (1-x)k_{B,n}\,]\,V_{Mix,corr}^{n-1} + \sum_{n=1}^{N} V_{Mix,corr}^{n-1} \sum_{r=1}^{n} \binom{n-1}{r} \left[x\,k_{A,n} + (1-x)\,k_{B,n}\right](\delta V)^{r} \approx P. \quad (9)$$

δV is therefore the deviation of the V_{Mix}-estimate, i.e. $V_{Mix,0}$, from its actual value. Such deviation from $V_{Mix,corr}$ partially compensates for neglecting in Eq. (8) both the ε-dependent contribution and the $O(x)$ term. In this light, δV affects the estimate of the excess properties of a solid mixing, predicted on the basis of its end-members. Using V_{Mix} and E_{Mix}, one is also able to calculate the enthalpy, i.e. $H_{Mix} = E_{Mix} + PV_{Mix}$.

Please, note that the arguments brought about above also hold for Helmholtz free energy, $F(V,T) = E(V,S) - TS$. If one uses $F(V,T)$, then Eq.(8) changes into

$$-\left(\frac{\partial F_{Mix}}{\partial V_{Mix}}\right)_{T} = P,$$

which is commonly used in practice, when vibration contributions to energy and entropy are also taken into account. Therefore, in this light, one can readily determine

$$\Delta V = V_{Mix} - x\,V_A - (1-x)V_B$$

$$\Delta E = E_{Mix} - x\,E_A - (1-x)E_B$$

$$\Delta F = F_{Mix} - x\,F_A - (1-x)F_B$$

and, combining the equation above,

$$\Delta H = \Delta E + P\Delta V$$

$$\Delta G = \Delta F + P\Delta V$$

where Δ refers to "excess" volume, energy, Helmholtz energy, enthalpy and Gibbs energy of a given solid mixing.

2.2 Error estimate

Using the V_{Mix}-estimate from Eq. (8) and the definition in Eq. (4.b), one can assess the legitimacy of the truncation of the summation in Eq. (4.a). In fact, one can write

$$\Delta Err_{Mix} = \sum_{n=1}^{N} V_{Mix,0}^{n} \sum_{r=1}^{n} \binom{n}{r} \left[\left(\frac{\delta_{A,0}}{V_{Mix,0}}\right)^{r} x\,k_{A,n} + \left(\frac{\delta_{B,0}}{V_{Mix,0}}\right)^{r} (1-x)\,k_{B,n}\right] =$$

$$\sum_{n=1}^{N} V_{Mix,0}^{n} \sum_{r=1}^{n} \binom{n}{r} \left[{\epsilon_A}^{r} x\,k_{A,n} + {\epsilon_B}^{r}(1-x)\,k_{B,n}\right] \quad (10)$$

where ΔErr_{Mix} is the $\varepsilon_{A,B}$-dependent contribution to energy. Therefore, it ensues from Eq. (10), Eq. (5) and neglecting *O(x)* that

$$\frac{\Delta Err_{Mix}}{Err_{Mix}} = \frac{\sum_{n=1}^{N} V_{Mix,0}^{n} \sum_{r=1}^{n} \binom{n}{r} [\epsilon_{A,0}{}^{r} x\, k_{A,n} + \epsilon_{B,0}{}^{r} (1-x)\, k_{B,n}]}{\sum_{n=0}^{N} [\, x k_{A,n} + (1-x) k_{B,n}\,]\, V_{Mix,0}^{n}} \approx \frac{\sum_{n=1}^{N} n [\epsilon_{A,0} x\, k_{A,n} + \epsilon_{B,0} (1-x)\, k_{B,n}] V_{Mix,0}^{n}}{\sum_{n=0}^{N} [\, x k_{A,n} + (1-x) k_{B,n}\,]\, V_{Mix,0}^{n}} =$$

$$\frac{\epsilon_{A,0} \sum_{n=1}^{N} n [x\, k_{A,n} + \epsilon_{B,0} / \epsilon_{A,0} (1-x)\, k_{B,n}] V_{Mix,0}^{n}}{\sum_{n=0}^{N} [\, x k_{A,n} + (1-x) k_{B,n}\,]\, V_{Mix,0}^{n}} \quad (11)$$

where we have assumed that $|\varepsilon_{A,0}| > |\varepsilon_{B,0}|$, for the sake of simplicity. From Eq. (11), one estimates a relative error as large as 0.2-0.3 ‰. Neglecting both ΔErr_{Mix} and $O(x)$ is a source of uncertainty, which is estimable for the former and unknown for the latter. Such uncertainty is partially compensated *via* $V_{Mix,0}$ (see Eq. (9)), i.e. the *estimate* of the actual mixing volume, namely $V_{Mix,corr}$. Therefore, a comparison is required between excess properties, predicted as discussed above, and previous excess data (experimental and theoretical) to assess the accuracy of the method presented.

2.3 Computational details

Energy was determined using static and vibrational contributions, for each solid mixing under study. The calculations were performed by the CRYSTAL14-code that exploits “Linear Combinations of Atomic Orbitals” [23]. We used a hybrid Hamiltonian, with Hartree-Fock/DFT rate, DFT functional and atomic basis set that were chosen differently from one case to another. The hybridization rate was determined to reproduce both unit cell volume and electronic energy gap, at room conditions. More details about the computing setup are reported in the “Results and discussion” section. The following tolerances that control the accuracy of the self-consistent cycles’ integrals were used: 10^{-9} for coulomb overlap; 10^{-9} for coulomb penetration; 10^{-9} for exchange overlap; 10^{-9} for exchange pseudo-overlap in direct space and 10^{-18} for exchange pseudo-overlap in reciprocal space; 10^{-10} a.u. threshold for SCF-cycles’ convergence. The shrinking factors of the reciprocal space (Monkhorst net, [24]) and of the secondary reciprocal space net (Gilat net, [25]) were set at 12 and 24, respectively. The vibrational energy was determined by combining atomic vibration frequencies of a harmonic model and standard statistical mechanics formalism, including zero point vibration and purely thermal contributions. The static $E(V)$-curves of the EMs were obtained by shrinking under a nominal P the cell volume up to about -10% with respect to the equilibrium

geometry determined at ambient pressure and 0 K. Then the vibration components of energy were calculated on the equilibrated structure and introduced. Eventually, the $F(V)$s of the end-members were determined by adding the configuration and vibration entropy contributions to $E(V)$s. The resulting $F(V)$s were expanded in polynomial bases of V_{Mix} and summed according to the Vegard's scheme, as discussed in the sections above. The degree of the polynomials used in this work varied from case to case (2nd and 3rd order polynomials have been mostly employed). V_{Mix} was determined by solving the fundamental equilibrium equation $-(\partial E/\partial V)_S = -(\partial F/\partial V)_T = P$, i.e. Eq.(8), for a given x value. Then, the lacking PV_{Mix} contribution was added to obtain the Gibbs free energy.

Among the V_{Mix}-solutions of Eq. (9), we chose the one fulfilling the following constraint: $V_{Mix,0}$ must be a real number such as $V_{Mix,0} > 0$.

3. Results and discussion

Five cases are investigated: C1) $Si_{1-x}Ge_x$ binary alloy, C2) wurtzite-like $Al_{1-x}Ga_xN$ pseudo-binary alloy, C3) its zinc-blende-like polymorph, C4) $Al_{1-x}Ga_xAs$ pseudo-binary alloy and C5) $(Mg_{1-x}Ca_x)_3Al_2(SiO_4)_3$ binary compound, involving two end-member garnets. The choice of such systems is due to the following reasons: C1 is a binary alloy with an experimentally measured large ΔV; C2-C3 are pseudo-binary alloys with experimentally determined very small ΔV; C4 is a pseudo-binary alloy with experimentally determined small but still positive ΔV; C5 provides an example of solid mixing other than an alloy, such that the atomic replacement takes place over a subset of the available crystal sites. In this view, C1-2-3-4-5 provide a coverage for experimentally measured and/or theoretically determined ΔV, ΔH and ΔG of systems that exhibit a variety of behaviours.

3.1. $Si_{1-x}Ge_x$ binary alloy

SiGe is an alloy with complete miscibility on the whole join, commonly used as a semiconductor material in integrated circuits and as a substrate for CMOS transistors in high-speed electronics and thermoelectric devices. The following basis set was used to model SiGe: Si, Si88-1111G [26]; Ge, triple-ξ basis set with polarization function with contraction scheme Ge9-7631-61G [27]. The PBESOL exchange correlation functional

[28], which we employed, is an extension to solid systems of the PBE exchange/correlation functional [29]. The used functional and a comparison between theoretical and observed properties are reported in Table 1.

Table 1

$Si_{1-x}Ge_x$ alloy: functionals used for exchange and correlation energies; hybridization rate, in %; lattice parameter, *a*; electron energy gap at Γ.

Compound	Exchange and correlation functional	HF/DFT Ratio(%)	*a*(Å) this study	E_{gap}(eV) this study	E_{gap} (eV) this study	*a*(Å) lit. [30]	E_{gap}(eV) lit. [31]
Si	PBESOL	15	5.4297	5.6627	1.190	5.4310	1.120
Ge	PBESOL	3	5.6483	5.6589	0.749	5.6562	0.744

$Si_{1-x}Ge_x$ crystallizes with diamond-like structure in the Space Group $Fd\bar{3}m$. In the present work, we have taken as a reference the experimental studies at ambient conditions of [30-32], which yield maximum excess volumes ranging from -0.4 up to 0.03%. We introduce the notions of i) "*literature data e.s.d*", defined as the estimated standard deviation (e.s.d) calculated with respect to the extant literature data (both experimental and theoretical), and ii) "*theoretical deviation*", calculated as the square root of the average square deviation of the extant literature data from our results. In so doing, we have that for ΔV the "theoretical deviation" is as large as 0.34 $Å^3$, versus a "literature data e.s.d" of 0.26 $Å^3$, i.e. our results exhibit a disagreement with respect to the extant data of the same order of magnitude of the internal scattering between excess volume values from literature. Figure 1 displays a comparison between ΔVs from this work and experimental measurements [30]. One observes that the occurrence of a small and negative ΔV is correctly predicted, and the average discrepancy between calculated and observed ΔV is about 0.34%.

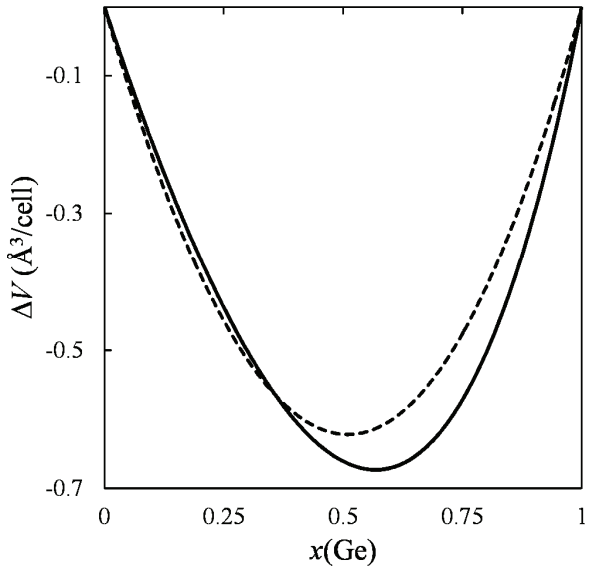

Fig. 1. $Si_{1-x}Ge_x$ alloy's excess volume, ΔV, at 300 K, as a function of the molar fraction of Ge. Solid line: this study; dashed line: experimental data from [30].

Binary alloys are often treated as regular solid solutions, whose excess enthalpy is modelled by $\Delta H = Wx(1-x)$, where W is the interaction parameter. Although the excess enthalpy of SiGe turns out to be slightly asymmetric, if we fit a regular model to our ΔH data we obtain a critical temperature $T_c \approx 435$ K ($T_c = W/2 \cdot k_B$), to be compared to T_c = 360 K, predicted by Qteish and Resta [33]. Figure 2 displays the excess Gibbs energy whose entropy term accounts for the configuration contribution, too. Values at 0 K, corresponding to static ΔH, are in agreement with the results by Bublik and Leikin [34].

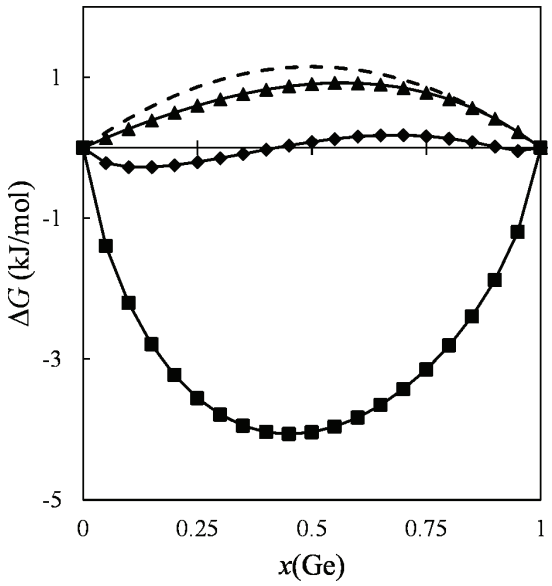

Fig. 2. $Si_{1-x}Ge_x$ alloy's excess Gibbs energy, ΔG, at 0, 300 and 1000 K as a function of the molar fraction of Ge. Triangles: this study, 0 K; diamonds: this study, 300 K; squares: this study, 1000 K; dashed line: data from [34] at 0 K.

Our results are qualitatively comparable with those in Figure 3 of [33], and a general accord reveals in terms of trend, with the largest discrepancy estimated at x = 0.5 of ≈ 0.3 kJ/mol, i.e. about 25%. Such a large disagreement reflects a likely low accuracy because of the difficulty to obtain numerical quantities from the related available figure of the aforementioned authors.

3.2 $Al_{1-x}Ga_xN$ ternary alloy (wurtzite-like structure)

Nitrides are widespread in two application areas: short-wavelength light emitters and high-power/high-temperature electronics. In particular, AlGaN is often used as a barrier material for nitride electronic and optoelectronic devices. AlGaN can crystallize in two structures: zinc-blende (space group, $F\bar{4}3m$) and wurtzite (space group, *P*63*mc*), the latter being the more stable phase at room conditions ($G_{Zn\text{-}BLEND}$-$G_{WURTZITE}$ ≈ 0.7 kJ/mol, at ambient pressure and temperature. See for instance [35]). In the present work, we

examined both cubic and hexagonal phases of $Al_{1-x}Ga_xN$. Reference structures and energy gap values for the end-members and along the AlN-GaN join are from [36-38].

In all our calculations related to $Al_{1-x}Ga_xN$, the aluminium was modelled by the Al 85-11G* basis set from [39], while gallium was described by the 86-4111d41G basis set [40]; N was represented by the 6-31d1G [41]. We used the M06 Minnesota 2006 global hybrid GGA-XC functional [42], resorting to hybridization rates of 23 and 19.5%, in AlN and GaN, respectively. Table 2 reports general information about the agreement between observed versus predicted properties.

Table 2

$Al_{1-x}Ga_xN$ alloy: functionals used for exchange and correlation energies; hybridization rate, in %; lattice parameter, *a* and *c*; electron energy gap at Γ. w = wurtzite-like structure; zb = zinc-blende-like structure.

Compound	Exchange and correlation functional	HF/DFT Ratio(%)	*a*(Å) this study	*c*(Å) this study	E_{gap} (eV) this study	*a*(Å) lit.	*c*(Å) lit.	E_{gap} (eV) exp.[b]
AlN – w1	M06	19.5	3.1176	4.9865	6.201	3.1120[a]	4.9813[a]	6.23[a]
GaN – w	M06	19.5	3.1904	5.1862	3.485	3.1875[a]	5.1837[a]	3.51[a]
AlN – zb	M06	19.5	4.3840	-	5.945	4.3800[b]	-	5.94[c]
GaN – zb	M06	19.5	4.5065	-	3.276	4.5200[b]	-	3.26[d]

[a] extrapolation to 0 K of experimental data by [36]
[b] Reference [43]
[c] Reference [44]
[d] Reference [45]

AlGaN-alloy's volume follows the Vegard's law, according to data reported in literature [46]. Our method predicts a very small ΔV, the largest deviation from linearity resulting in ≈ -0.04 $Å^3$/cell at *x*(Ga) = 0.5, as one infers by Figure 3, in agreement with earlier first-principles calculations [47].

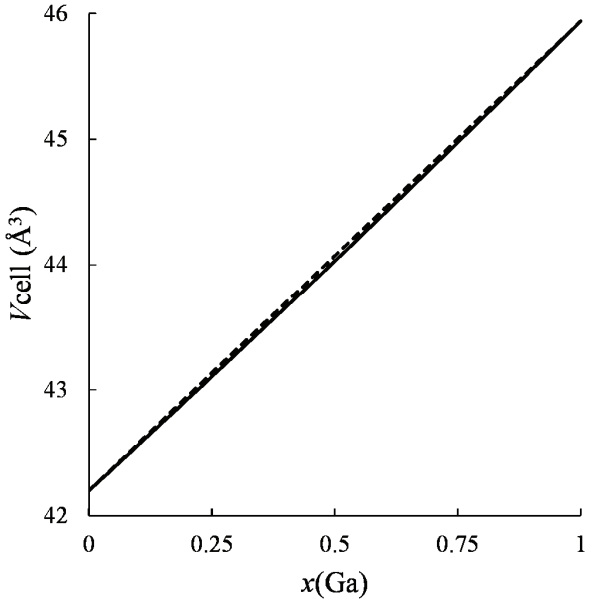

Fig. 3. Wurtzite-like $Al_{1-x}Ga_xN$ alloy's unit cell volume, *V*, as a function of the molar fraction of Ga. Calculated volumes (solid line) and *V*s predicted using the Vegard's law and our EMs' cell parameters.

The "theoretical deviation" of our ΔVs is ≈ 0.04 Å^3, versus a "literature data e.s.d." of ≈ 0.03 Å^3. In Figure 4 the excess Gibbs energy curves of wurtzite-like AlGaN alloy at 1200, 1600 and 2000 K are shown and compared with results obtained by the DLP model [5]. The average discrepancy between our model and DLP is ≈ 3.0%, 2.3% and 1.9% at 1200, 1600 and 2000 K, respectively.

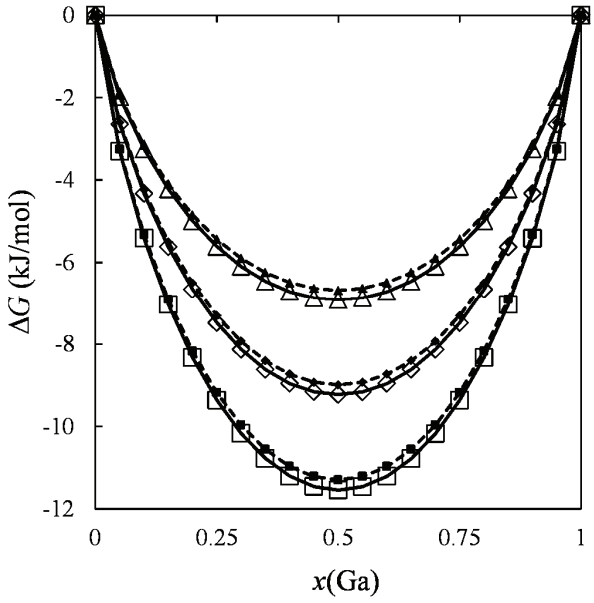

Fig. 4. Wurtzite-like $Al_{1-x}Ga_xN$ alloy's excess Gibbs energy, ΔG, at various temperatures as a function of the molar fraction of Ga. Our ΔGs (empty symbols and solid lines) are compared to those calculated by means of the DLP model [5] (filled symbols and dashed lines). Triangles: 1200 K; diamonds: 1600 K; squares: 2000 K.

Our results are also qualitatively consistent with those reported in Figure 3 by Simonya et al. [35], who calculated the Gibbs energy of mixing as a function of *T* by means of the DLP model (mean discrepancy with our data ≈ 7%).

3.3 $Al_{1-x}Ga_xN$ ternary compound (zinc-blende-like structure)

The end-members AlN and GaN of $Al_{1-x}Ga_xN$ (cubic) were modelled using the setup employed for the hexagonal polymorph. Reference experimental data for cell edge and electron energy gap are provided by [32] and [48-51].

Our cell volume exhibits a slight underestimation with respect to the observed values that follow a Vegard-like trend, as reported by Figure 5, in agreement with first-

principles calculations [50]. The “literature data e.d.s” and “theoretical deviation” of *V* are as large as ≈ 0.79 and 0.69 Å^3, respectively.

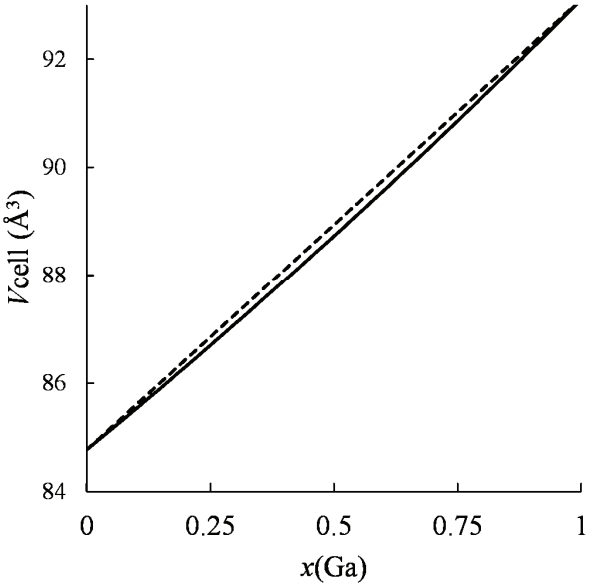

Fig. 5. Zinc-blende-like $Al_{1-x}Ga_xN$ alloy’s unit cell volume, *V*, as a function of the molar fraction of Ga. Calculated volumes (solid line) and *V*s predicted using the Vegard’s law and our EMs’ cell parameters (dashed line).

In Figure 6 mixing enthalpy and Gibbs energy curves are displayed. They show a satisfactory agreement with results from [51] (0 K; discrepancy ≈ 5%) and with those by the DLP model of Stringfellow [5]; in the latter case, we observe an average discrepancy of 1.9%, 1.4% and 1.1% at 1200, 1600 and 2000 K, respectively.

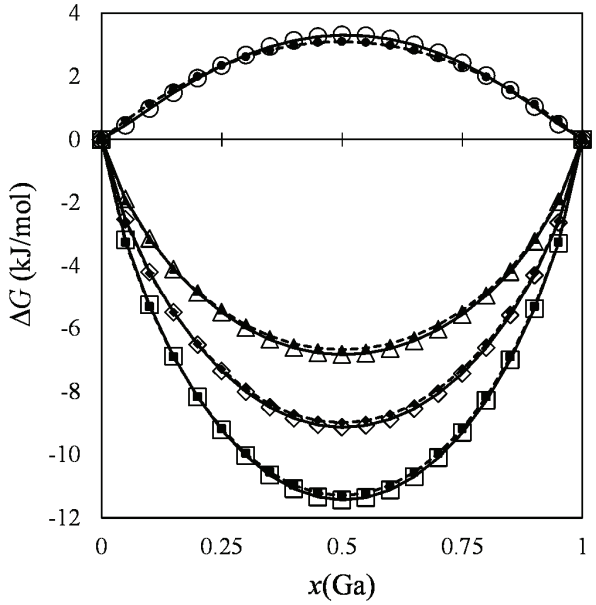

Fig. 6. Zinc-blende-like $Al_{1-x}Ga_xN$ alloy's excess Gibbs energy, ΔG, at various temperatures as a function of the molar fraction of Ga. Our ΔGs (empty symbols) are compared to those calculated by the Stringfellow's DLP model [5] (filled symbols) and, for T = 0 K, to those (filled symbols) in [51]. Triangles: 1200 K; diamonds: 1600 K; squares: 1800; circles: 0 K.

A qualitative agreement is observable between our ΔGs and those shown by Figure 3 in [35], which does not report numerical data. By way of example, at x = 0.5 the discrepancy between our ΔG and the value in [35] is estimated ≈ 12%.

3.4 $Al_{1-x}Ga_xAs$ ternary compound (zinc-blende-like structure)

$Al_xGa_{1-x}As$ crystallizes in the space group $F\bar{4}3m$. Exchange and correlation energies are modelled by the B1WC functional [52], i.e. a combination of WCGGA [53] and PWGGA [29], as summarized in Table 3. Experimental geometry data are from [32].

Table 3

$Al_{1-x}Ga_xAs$ alloy: functionals used for exchange and correlation energies; hybridization rate, in %; lattice parameter, *a*; electron energy gap at Γ.

Compound	Exchange functional	Correlation functional	HF/DFT Ratio(%)	*a*(Å) this study	E_{gap} (eV) this study	*a*(Å) exp.[a]	E_{gap} (eV) exp.[b]
AlAs	WCGGA	PWGGA	11	5.6627	2.183	5.6601	2.240
GaAs	WCGGA	PWGGA	1	5.6589	1.538	5.6515	1.519

[a] extrapolation to 0 K of data by [32].
[b] extrapolation to 0 K of data by [48].

The cell edge, *a*, is parametrised as a function of the composition, in terms of the following equation [32]

$a(\text{Å}) = xa(\text{AlAs})+(1-x)a(\text{GaAs})+Wx(1-x)$

where the value of the bowing parameter, W, is 0.0011 Å. Our modelling, at room conditions, yields W≈ 0.0013 Å, in keeping with the experimental determination. Figure 7 shows that our predictions of excess lattice parameter are in agreement with the results reported in literature [54], in terms of an average absolute discrepancy of about 2.1%.

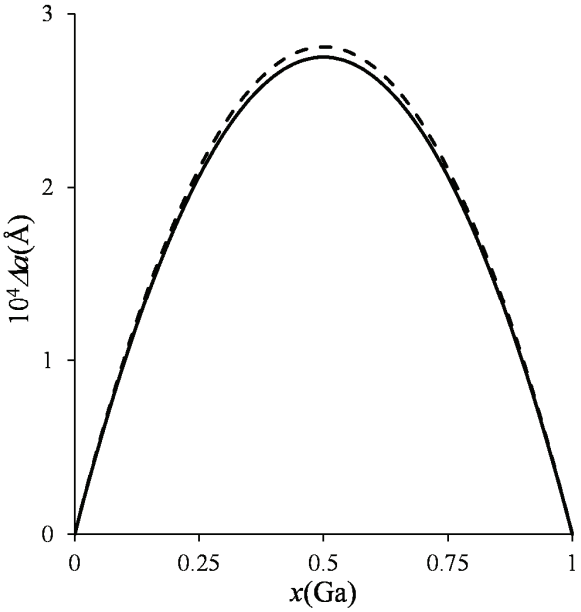

Fig. 7. $Al_{1-x}Ga_xAs$ alloy's excess cell edge, Δ*a*, at 300 K as a function of the molar fraction of Ge. Solid line: this study; dashed line: data from [54].

In Figure 8 the excess Gibbs energy curves at 0, 300, 1000 and 1500 K are plotted.

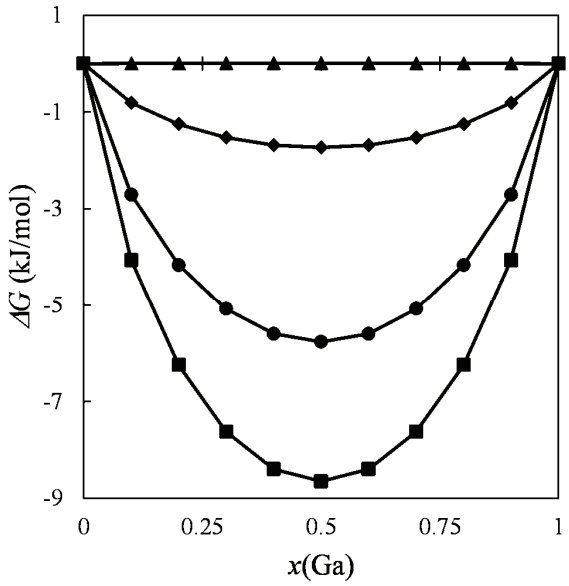

Fig. 8. Calculated ΔG of mixing for $Al_{1-x}Ga_xAs$ as a function of the molar fraction of Ga. Triangles: 0 K; diamonds: 300 K; circles: 1000 K; squares: 1500 K.

The solid solution exhibits a symmetric behaviour, in agreement with expectations according to data reported in [34]. The obtained enthalpy of mixing is practically negligible (maximum $\Delta H \sim 3 \cdot 10^{-3}$ kJ/mol) and ΔG is governed mostly by the pure configuration entropy contribution.

3.5 $(Mg_{1-x}Ca_x)_3Al_2(SiO_4)_3$ garnet: pyrope-grossular join

The $(Mg_{1-x}Ca_x)_3Al_2(SiO_4)_3$ mixing has roused much attention in the Earth Sciences, and a critical review on the still-debated excess thermodynamic properties of such solid solution is provided by Dove and Geiger [55]. In the present work, reference geometry was taken from [56] and exchange-correlation energy was modelled by the M06 Minnesota 2006 global hybrid GGA-XC functional [42] with hybridization ratios of 28.5 and 27% for pyrope and grossular, respectively (Table 4).

Table 4

$(Mg_{1-x}Ca_x)_3Al_2Si_3O_{12}$ garnet solid solution: functionals used for exchange and correlation energies; hybridization rate, in %; lattice parameter, *a*; electron energy gap at Γ.

Compound	Exchange and correlation functional	HF/DFT Ratio(%)	*a*(Å) this study	E_{gap} (eV) this study	*a*(Å) exp. [56]	E_{gap}(eV) exp.
$Mg_3Al_2Si_3O_{12}$	M06	28.5	11.4542	8.79	11.457(1)	-
$Ca_3Al_2Si_3O_{12}$	M06	27	11.8534	8.57	11.852(1)	-

Extant Δ*V*s yield a "literature data e.s.d" of ≈ 1.14 Å^3, versus a "theoretical deviation" of ≈ 1.05 Å^3. Figure 9 shows a comparison between our predicted Δ*V*s and measurements by Newton et al. [57] and reveals an average absolute discrepancy of 10% (i.e. an average deviation of 0.35 Å^3). Larger average absolute discrepancies of 40% (average absolute difference of ≈ 1.3 Å^3) and 37% (average absolute difference of 1.2 Å) are observed, comparing our excess volumes with those in [58] and [56], respectively. Note that the maximum Δ*V* discrepancy between our results and literature's is ≈ 1-1.3 Å^3, corresponding to ≈ 0.20%-0.35% unit cell volume, i.e. a comparatively small quantity with respect to *V*.

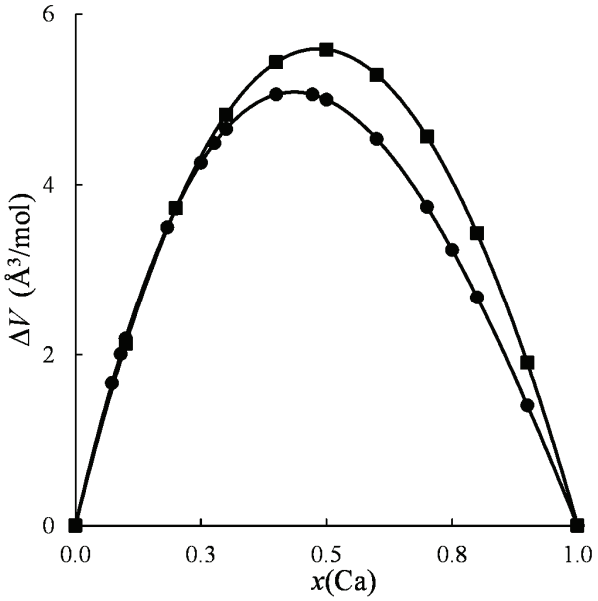

Fig. 9. $(Mg_{1-x}Ca_x)_3Al_2Si_3O_{12}$ solid solution excess volume, ΔV, as a function of the molar fraction of Ca. Squares: this study (at 0 K); circles: experimental room conditions data from [57].

[59] provide excess volume values that are in contrast with the extant ones in literature, giving significantly larger ΔVs (even three times as large as those from the abovementioned references). In this view, we are inclined to leave the determinations by [59] aside.

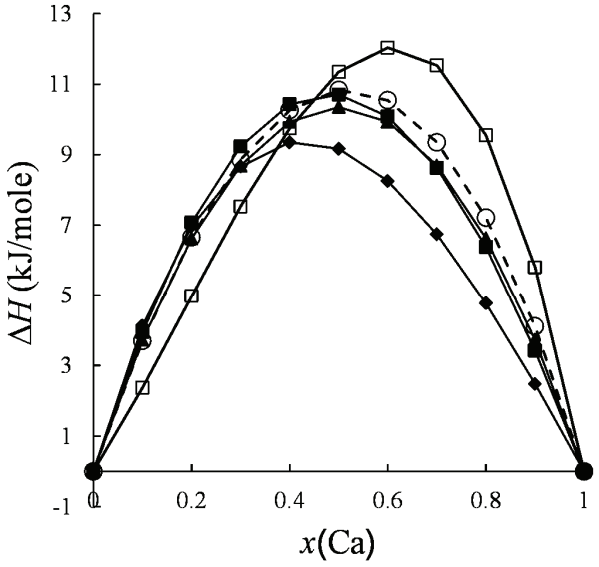

Fig. 10. $(Mg_{1-x}Ca_x)_3Al_2Si_3O_{12}$ solid solution excess enthalpy, ΔH, as a function of the molar fraction of Ca. Filled squares: this study at 300 K; empty circles: Margules fitting of our data at 300 K; filled diamonds: [57]; filled triangles: [61]; open squares: [60].

In Figure 10, we report ΔH-curves from literature, in comparison with ours, at room conditions. Considering the experimental uncertainty between observations from different authors, our results are in general agreement with measurements. In particular, in the region $0.4<x(Ca)<1$ our model provides an excess enthalpy curve that lies between those by [57] and [60], with an average discrepancy of 15% and 30% respectively. Our ΔHs fully match data by Hodges and Spear [61] over the whole x(Ca)-range, with an average discrepancy of ≈ 5%. Eventually, in the region $x(Ca)<0.4$, our excess enthalpy data agree with all earlier measurements. Altogether, ΔH yields a "literature data e.s.d." of 2.1 kJ/mol, versus a "theoretical deviation" of 1.4 kJ/mol, namely our modelling matches well average experimental data.

4. Conclusions

A method for calculation of the excess volume, enthalpy and Gibbs energy of binary/pseudo-binary joins has been developed, using the $E(V,S)$ and $F(V,T)$ state functions of the end-members only. On one hand, this remarkably relieves heavy

computing to model solid mixings; on the other hand, it provides an advancement with respect to the classic Vegard's law, allowing prediction of excess quantities. The present approach pivots around the fundamental observable V_{Mix} (equilibrium volume of a solid solution), which is determined by Eq. (8). The capacity of the method presented herein to reproduce observations is assessed by a comparison between our predictions and experimental/theoretical data for five cases of previously studied solid solutions, at room pressure: $Si_{1-x}Ge_x$, $Al_{1-x}Ga_xN$ (cubic), $Al_{1-x}Ga_xN$ (hexagonal), $Al_{1-x}Ga_xAs$, $(Mg_{1-x}Ca_x)_3Al_2(SiO_4)_3$. They provide widely investigated joins and cover a range of solid mixings from alloys to silicate compounds. The earlier measured and calculated excess volume, enthalpy and Gibbs energy values from literature are often scattered. To take this into account, we compare the "literature data e.s.d", namely the e.s.d calculated by data of literature, with the "theoretical deviation", corresponding to the square root of the mean square deviation of our excess data from the extant ones found in literature. In so doing, we observe that the "literature data e.s.d" to "theoretical deviation" ratio is very close to unity, thus proving that our predictions agree with previous determinations, on average. ΔV, ΔH and ΔG exhibit average discrepancies between our results and earlier data of some 5, 10, and 12%, respectively. Such figures can be temporarily taken as first approximation estimates of the method's accuracy, until further comparisons with experimental/theoretical data will be available. On one hand, the present model complements Stringfellow's[5], which is efficient and simple, but difficult to be transferred to high pressure investigations and limited to symmetric solid solutions. On the other hand, our approach makes it possible to model solid mixings at any condition by directly using the energy of the EMs, thus drastically reducing the difficulty to perform calculations. Further work will be devoted to extending the present technique in two respects: 1) high pressure studies of solid solutions at extreme conditions; 2) multi-component systems, beyond binary joins.

Ackowledgements

The present study was granted by the “PRIN2017-2017L83S77” project of the Italian Ministry for Education, University and Research (MIUR). The authors are grateful to an anonymous referee for useful suggestions that improved the manuscript and to Dr. L.J. Kurilla for linguistic revision of the text.

References

[1] L. Vegard, Die Konstitution der Mischkristallen und die Raumfullung der Atome, Z. Phys. 5 (1921) 17-26.

[2] K.T. Jacob, S. Raj and L. Rannesh, Vegard’s law: a fundamental relation or an approximation? Int. J. Mat. Res. 98 (2007) 776-779.

[3] H.A. Moreen, R. Taggart, D.H. Polonis, A model for the prediction of lattice parameters of solid solutions, Metall. Trans. 2 (1971) 265-268.

[4] A.R. Denton and N.W. Ashcroft, Vegard’s law, Phys. Rev. A. 43 (1991) 3161-3164.

[5] G.B. Stringfellow, Calculation of ternary and quaternary III-V phase diagrams, J. Cryst. Growth 27 (1974) 21-34.

[6] A. Gonis, Green Functions for Ordered and Disordered Systems, Studies in Mathematical

Physics, edited by van Groesen E. and de Jager E. M., Vol. 4, North-Holland, Amsterdam, 1992.

[7] J.W. Connolly and A.R. Williams, Density-functional theory applied to phase transformations in transition-metal alloys, Phys. Rev. B 27 (1983) 5169-5172.

[8] J.E. Mayer and E. Montroll, Molecular Distribution, J. Chem. Phys. 9 (1941) 2-16.

[9] Q. Wu, B. He, T. Song, J. Gao and S. Shi, Cluster expansion method and its application in computational materials science, Comp. Mat. Sci. 125 (2016) 243-254.

[10] A. Bosenick, M.T. Dove, E.R. Myers, E.J. Palin, C.I. Sainz-Diaz, B.S. Guiton, M.C. Warren and M.S. Craig, Computational methods for the study of energies of cation distributions: applications to cation-ordering phase transitions and solid solutions, Mineral. Mag. 65 (2001) 193-219.

[11] M.C. Warren, M.T. Dove, E.R. Myers, A. Bosenick, E.J. Palin, C.I. Sainz-Diaz, and Guiton, B. Monte Carlo methods for the study of cation ordering in minerals, Mineral. Mag. 65 (2001) 221-248.

[12] M. Merli, L. Sciascia, A. Pavese, V. Diella, Modelling of thermo-chemical properties over the sub-solidus MgO–FeO binary, as a function of iron spin configuration, composition and temperature, Phys. Chem. Miner. 42 (2015) 347-362.

[13] M. Merli, C. Bonadiman, V. Diella, L. Sciascia and A. Pavese, Fe-periclase reactivity at Earth's lower mantle conditions: Ab-initio geochemical modelling. Geochim. Cosmochim. Ac. 214 (2017) 14-29.

[14] L. Bellaiche, D. Vanderbilt, Virtual crystal approximation revisited: Application to dielectric and piezoelectric properties of perovskites, Phys. Rev. B 61 (2000) 7877-7782.

[15] T.G. Dargam, R.B. Capaz, and B. Koiller, Critical analysis of the virtual crystal approximation, Braz. J. Phys. 27/A (1997) 299-304.

[16] M. H. F. Sluiter and Y. Kawazoe, Prediction of the mixing enthalpy of alloys, Europhys. Lett. 57 (2002) 526–532.

[17] L. Zhang, Thermodynamic properties calculation for MgO–SiO_2 liquids using both empirical and first-principles molecular simulations, Phys. Chem. Chem. Phys. 13 (2011) 21009-21015.

[18] J.-P. Harvey, A. Gheribi and P.D. Asimow, A self-consistent optimization of multicomponent solution properties: Ab initio molecular dynamic simulations and the MgO-SiO_2 miscibility gap under pressure, Geochim. Cosmochim. Ac. 161 (2015) 146-165.

[19] D. Belmonte, G. Ottonello, M. Vetuschi Zuccolini and M. Attene, The system MgO-Al_2O_3-SiO_2 under pressure: A computational study of melting relations and phase diagrams, Chem. Geol. 461 (2017) 54-64.

[20] D. Belmonte, G. Ottonello and M. Vetuschi Zuccolini, Ab initio-assisted assessment of the CaO-SiO_2 system under pressure, Calphad 59 (2017) 12-30.

[21] Myhill, R. The elastic solid solution model for minerals at high pressures and temperatures, Contrib. Mineral. Petrol. 173 (2018) 1-17.

[22] M. Gottschalk, Beyond the Margules equation: a universal thermodynamic equation for solid solutions including coupled substitution, long- and short-range order, Eur. J. Mineral. 28 (2016) 219-244.

[23] R. Dovesi, V.R. Saunders, C. Roetti, R. Orlando, C.M. Zicovich-Wilson, F. Pascale, B. Civalleri, K. Doll, N.M. Harrison, I.J. Bush, Ph. D'Arco, M. Llunell, M. Causà and Y. Noël, CRYSTAL14 *User's manual,* University of Torino, Torino, 2014.

[24] H.J. Monkhorst and J.D. Pack, Special points for Brillouin-zone integrations, Phys. Rev. B, 13 (1976) 5188-5192.

[25] G. Gilat and L.J. Raubenheimer, Accurate numerical method for calculating frequency-distribution in solids, Phys. Rev. 144, (1966) 390-395.

[26] A.R. Porter, M.D. Towler and R.J. Needs, Muonium as a hydrogen analogue in silicon and germanium; quantum effects and hyperfine parameters, Phys. Rev. B 60 (1999) 13534-13546.

[27] E. Ruiz, M. Llunell and P. Alemany, Calculation of exchange coupling constants in solid state transition metal compounds using localized atomic orbital basis sets, J. Solid State Chem. 176 (2003) 400-411.

[28] J.P. Perdew, A. Ruzsinszky, G.I. Csonka, O.A. Vydrov, G.E. Scuseria, L.A. Constantin, X. Zhou and K. Burke, Restoring the Density-Gradient Expansion for Exchange in Solids and Surfaces, Phys. Rev. Lett., 100 (2008) 136406-4.

[29] J.P. Perdew, J.A. Chevary, S.H. Vosko, K.A. Jackson, M.R. Pederson, D.J. Singh, and C. Fiolhais, Atoms, molecules, solids and surfaces: applications of the generalized gradient approximation for exchange and correlation, Phys. Rev. B 46 (1992) 6671-6687.

[30] J.P. Dismukes, L. Ekstrom, E.F. Steigmeier, I. Kudman and D.S. Beers, Thermal and Electrical Properties of Heavily Doped Ge-Si Alloys up to 1300°K, J. Appl. Phys. 35 (1964) 2899-2907.

[31] S. Adachi, Properties of Semiconductor Alloys: Group-IV, III-V, and II-VI Semiconductors, Wiley, Chichester, 2009.

[32] C. Ferrari and C. Bocchi, Characterization of Semiconductor Heterostructures and Nanostructures, Elsevier, Amsterdam, 2008.

[33] A. Qteish and R. Resta, Thermodynamic properties of Si-Ge alloys, Phys. Rev. B 37 (1988) 6983-6990.

[34] V.T. Bublik and V.N. Leikin, Calculation of the Pseudo-binary Alloy Semiconductor Phase Diagrams, Phys. Status Solidi (a) 46 (1978) 365-372.

[35] A.K. Simonya, K.M. Gambaryan, V.M. Aroutiounian, Nanostructures Nucleation Features and Miscibility Analysis in Zinc-Blend and Wurtzite GaN-InN-AlN Material System, J. Nanosci. Tech. 3 (2017) 253-255.

[36] I. Vurgaftman, R.C. Meyer, Band parameters for nitrogen-containing semiconductors, J. Appl. Phys. 94 (2003) 3675-3696.

[37] H. Schulz and K.H. Thiemann, Crystal structure refinement of AlN and GaN, Solid State Commun. 23 (1977) 815-819.

[38] D. Chandrasekhar, D.J. Smith, S. Strite, M.E. Lin and H. Morko, Characterization of Group III-nitride semiconductors by high-resolution electron microscopy, J. Cryst. Growth 152 (1995) 135-142.

[39] M. Catti, G. Valerio, R. Dovesi and M. Causa'. `Quantum-mechanical calculations of the solid-state equilibrium MgO + alpha-Al_2O_3 $MgAl_2O_4$ (spinel) versus pressure, Phys. Rev. B 49 (1994) 14179-14187.

[40] R. Pandey, J.E. Jaffe, N.M. Harrison, Ab-initio study of high-pressure phase-transition in GaN, J. Phys. Chem. Solids 55 (1994) 1357-1361.

[41] C. Gatti, V.R. Saunders, C. Roetti, Crystal-field effects on the topological properties of the electron-density in molecular-crystals - the case of urea, J. Chem. Phys. 101 (1994) 10686-10696.

[42] Y. Zhao and D.G. Truhlar, The M06 Suite of Density Functionals for Main Group Thermochemistry, Thermochemical Kinetics, Noncovalent Interactions, Excited States, and Transition Elements: Two New Functionals and Systematic Testing of Four M06-Class Functionals and 12 Other Functionals, Theor. Chem. Acc. 120 (2008) 215-241.

[43] A. Trampert, O. Brandt and K.H. Ploog, in: *Semiconductors and Semimetals* Vol. 50, Academic, San Diego, 1998.

[44] W.J. Fan, M.F. Li, T.C. Chong and J.B. Xia, Electronic properties of zinc-blende GaN, AlN, and their alloys $Ga_{1-x}Al_xN$, J. Appl. Phys. 79 (1996) 188-194.

[45] E. Martinez-Guerrero, C. Adelmann, F. Chabuel, J. Simon, N.T. Pelekanos, G. Mula, B. Daudin, G. Feuillet, and H. Mariett, Self-assembled zinc blende GaN quantum dots grown by molecular-beam epitaxy, Appl. Phys. Lett. 77 (2000) 809-811.

[46] Y. Koide, H. Itoh, N. Sawaki, I. Akasaki and M. Hashimoto, Epitaxial Growth and Properties of AlxGa1-xN by MOVPE. J. Electrochem. Soc. 133 (1986) 1956-1960.

[47] Z. Dridi, B. Bouhafs, P. Ruterana, First-principles investigation of lattice constants and bowing parameters in wurtzite $Al_xGa_{1-x}N$, $In_xGa_{1-x}N$ and $In_xAl_{1-x}N$ alloys, Semicond. Sci. Tech. 18 (2003) 850–856.

[48] I. Vurgaftman, J.R. Meyer and L.R. Ram-Mohan, Band parameters for III--V compound semiconductors and their alloys, J. App. Phys. 89 (2001) 5815-5875.

[49] K. Kim, S. Limpijumnong,W.R.L. Lambrecht, B. Segall, in: III–V Nitrides, in: F.A. Ponce, T.D. Moustakas, I. Akasaki, B.A. Monemar (Eds.), Materials Research Society Symposium Proceedings, 449, 1996, pp 929-934.

[50] Z. Dridi, B. Bouhafs, P. Ruterana, First-principles study of cubic $Al_xGa_{1-x}N$ alloys, Comp. Mater. Sci. 33 (2005) 136–140.

[51] S.Y. Karpov, N.I. Podolskaya, and I.A. Zhmakin, Statistical model of ternary group-III nitrides, Phys. Rev. B 70 (2004) 235203-10.

[52] D.I. Bilc, R. Orlando, R. Shaltaf, G.M. Rignanese, J. Iniguez and Ph. Ghosez, Hybrid exchange-correlation functional for accurate prediction of the electronic and structural properties of ferroelectric oxides, Phys. Rev. B 77 (2008) 165107-13.

[53] Z. Wu, and R.E. Cohen, More accurate generalized gradient approximation for solids, Phys. Rev. B 73 (2006) 235116-6.

[54] D. Zhou and B. Usher. Deviation of the AlGaAs lattice constant from Vegard's law, J. Phys. D Appl. Phys. 34 (2001) 1461-1465.

[55] M.T. Dove and C.A. Geiger, Scaling of thermodynamic mixing properties in garnet solid solutions, Phys. Chem. Miner. 28 (2001) 177-187.

[56] J. Ganguly, W. Cheng and H.St.C. O'Neill, Syntheses, volume, and structural changes of garnets in the pyrope-grossular join; implications for stability and mixing properties. Am. Mineral. 78 (1993) 583–593.

[57] R.C. Newton, T.V. Charlu, and O.J. Kleppa, Thermochemistry of high pressure garnets and clinopyroxenes in the system CaO-MgO-$Al2O_3$-SiO_2, Geochim. Cosmochim. Ac. 41 (1977) 369-377.

[58] A. Bosenick and C.A. Geiger, Powder X ray diffraction study of synthetic pyrope-grossular garnets between 20 and 295 K, J. Geophys. Res. 107 B10 (1997) 22649-22657.

[59] W. Du, S.M. Clark and D. Walker, Excess mixing volume, microstrain, and stability of pyrope-grossular garnets, Am. Mineral. 101 (2016) 193-204.

[60] R.G. Berman, Mixing properties of Ca-Mg-Fe-Mn garnets, Am. Mineral. 75 (1990) 328-344.

[61] K.V. Hodges and F.S. Spear, Geothermometry, geobarometry and the Al_2SiO_5, triple point at Mt. Moosilauke, New Hampshire, Am. Mineral. 67 (1982) 1118-1134.

Declaration of interests

☒ The authors declare that they have no known competing financial interests or personal relationships that could have appeared to influence the work reported in this paper.

☐The authors declare the following financial interests/personal relationships which may be considered as potential competing interests: